Mon. Not. R. Astron. Soc. **266,** 399–411 (1994)

The physical conditions within dense cold clouds in cooling flows

G. J. Ferland,[1] A. C. Fabian[2] and R. M. Johnstone[2]
[1]*Department of Physics and Astronomy, University of Kentucky, Lexington KY 40506, USA*
[2]*Institute of Astronomy, Madingley Road, Cambridge CB3 0HA*

Accepted 1993 August 9. Received 1993 August 6; in original form 1993 May 25

ABSTRACT

Cold condensations are inferred to occur throughout X-ray-emitting cooling flows. This paper investigates the physical conditions within these clouds. Photoionization by the diffuse continuum produced by the surrounding hot gas heats and ionizes the surface of the cloud to intermediate temperatures (typically 6000 K) and low ionization (the main species present are atomic or singly ionized). A thermal front occurs at a depth of roughly 6×10^{15} cm (which corresponds to a hydrogen column density of $\sim 3 \times 10^{17}$ cm^{-2}), where the conditions change over to those similar to the cold phase of the interstellar medium. The gas within is predominantly cold (well below 100 K), molecular, and X-ray-heated. Molecular hydrogen forms via H^- in the dust-free conditions expected for gas that has rapidly cooled from X-ray-emitting temperatures. The Lyman–Werner bands of H_2 become optically thick, and the hydrogen becomes highly molecular. Eventually, the cloud becomes self-shielded as the result of a combination of the photoelectric opacity of atomic carbon and Rayleigh scattering, and carbon monoxide forms. Cooling by rotational transitions of CO brings the temperature of the core of the cloud to that of the cosmic background. We argue that this is the most likely state of any cloud with sufficient column density to be self-shielded from the diffuse X-ray continuum. Fragmentation in this core may produce a population of substellar objects.

Key words: molecular processes – galaxies: clustering – cooling flows – intergalactic medium.

1 INTRODUCTION

Cooling flows in clusters of galaxies deposit large quantities of cooled gas around the central galaxy at rates of tens to hundreds of solar masses per year (Fabian, Nulsen & Canizares 1984, 1991; Sarazin 1986). The final fate of the cooled gas is uncertain. It may just accumulate as cold dense clouds, such as have been recently inferred to occur in these regions from X-ray absorption studies (White et al. 1991) and 21-cm HI observations (Jaffe 1990), and/or it may collapse to form stars. The conditions within the cores of clusters are so very different from those in our own interstellar medium that the initial mass function (IMF) of the stars formed may be different from that in the solar neighbourhood. In particular, it has been suggested that the IMF is biased to low-mass stars (Cowie & Binney 1988; Fabian, Nulsen & Canizares 1982; Sarazin & O'Connell 1983). This then explains why little star formation is ever seen around central cluster galaxies: the stars that are formed are too faint to be easily detected.

The main differences between the intracluster medium in a cooling flow and the interstellar medium of our Galaxy are that (i) the former has a much higher mean pressure by factors of 100–1000; (ii) the immediately cooled gas is unlikely to contain dust, since it was previously above 10^7 K where the dust is destroyed by sputtering (see Draine & Salpeter 1979); and (iii) large molecular clouds cannot exist at large distances from the central cluster galaxy, since they would be destroyed by viscous drag as they fell through the hot medium (see Fabian et al. 1991). In order to collapse to form a star, the mass of a cloud must exceed a critical mass, at which the self-gravity of the cloud equals the pressure forces acting to resist collapse. If the pressure is purely thermal (as assumed here) then the critical mass is the Jeans mass. In this paper, we investigate the structure of cold gas clouds in the conditions of a cooling flow, and show that they can cool to such low temperatures that the Jeans mass can be less than a solar mass. The calculations are carried out for a typical cloud at a distance of about 100 kpc from the central galaxy. We are not concerned here with the optical line nebulosities often observed at the centres of cooling flows.

It is not clear how the Jeans mass is related to the final mass spectrum of stars. If most of the gravitational energy released during collapse of a region can be radiated away,

further fragmentation may take place (Hoyle 1953; Low & Lynden-Bell 1975; Rees 1976). As the gas cloud collapses, the density rises and the Jeans mass reduces, so making regions that are slightly denser, but were below the initial Jeans mass, now above the reduced Jeans mass. This process will continue to lower the mass of the fragments until the clouds become optically thick so that they no longer remain isothermal. Fragments might also coalesce or accrete the surrounding gas. This suggests that the Jeans mass is likely to be the upper mass limit of the resultant IMF. Clouds that have a total mass below their Jeans mass will not collapse under their own gravity, unless they can cool or accrete more mass. Clouds that are above the Jeans mass are presumed to collapse and form stars.

Whether stars form with masses considerably above the Jeans mass depends upon whether gas clouds of high mass can survive in a cooling flow without being shredded by their motion relative to the hot gas (and other processes) and upon the role of magnetic fields and angular momentum. Tangled magnetic fields are necessary in order to give small gas clouds some cohesion in the flow and to suppress thermal conduction. They can increase the critical mass for gravitational collapse if their pressure becomes significant relative to the thermal pressure of the cold gas. We ignore these effects here, although we note the uncertainty that they introduce into our final results. Magnetic fields may be of considerable importance for star formation in the core of a cooling flow (Richer et al. 1993).

In Section 2, we discuss the environment of a cooling flow. The pressure and radiation field expected there are used as the boundary and input conditions for our computations of the physical state (temperature, ionization and composition) of the cold gas. The modifications needed for the radiative equilibrium code CLOUDY at the expected low temperatures are discussed in Appendix A. In Appendix B we present a test calculation for the Orion Photo Dissociation Region as a check on the results. The results for the cooling flow (computed with CLOUDY, version 84.00) are given in Section 3, where we show that much of the cloud becomes molecular and very cold. This then allows us to compute the Jeans mass of the clouds in a straightforward manner, and to show that low-mass stars are a likely endpoint if they undergo gravitational collapse.

2 THE COOLING FLOW ENVIRONMENT

X-ray images of clusters of galaxies show that the majority have a surface brightness profile, within the central few hundred kpc, that is much more peaked than expected from a simple isothermal halo (Edge, Stewart & Fabian 1992). Either the mean gas temperature is observed to drop in this region, or X-ray-emitting components cooler than the temperature of the bulk of the cluster gas are observed (Mushotzky 1992). Those few clusters that do not have a peaked profile are invariably clusters that have two giant elliptical galaxies, as is seen in the Coma cluster, rather than a single central dominant galaxy. These may be cases where two clusters of roughly similar mass have recently merged and the cooling flows of each have become spread out over a much larger region in the middle of the merged cluster.

The radiative cooling time of the hot intracluster gas, $t_{\rm cool}$, reduces sharply as the centre of the cluster is approached. Within a radius $r_{\rm cool}$ defined where $t_{\rm cool} = H_0^{-1}$ (the Hubble time), typically 100–200 kpc, most of the gas loses its thermal energy to radiation, and a cooling flow develops. Gas flows inward to maintain the pressure necessary to support the weight of the overlying gas.

To first order, the rate at which gas cools at radius r within $r_{\rm cool}$, $\dot{M}$, is simply related to the luminosity within r,

$$\dot{M} = \frac{2}{5}\frac{\mu m_{\rm H} L_{\rm cool}}{kT_{\rm X}}, \qquad (1)$$

where $T_{\rm X}$ is the initial high temperature of the gas, and $\mu m_{\rm H}$ is the mean molecular weight. This simple estimate can be corrected for the luminosity contributed by the gravitational work done on the flow. In practice, it reduces the mass deposition rate inferred from the observed luminosity by up to a factor of 2 from the value obtained using equation (1).

Detailed studies of the observed X-ray luminosity profile of cooling flows show that $\dot{M}$ is not constant with radius, but that the integral mass deposition rate within radius r is

$$\dot{M}(<r) \propto r \qquad (2)$$

(Fabian et al. 1984; Thomas, Fabian & Nulsen 1987; White & Sarazin 1987), so that the cooled gas is deposited in a distributed manner within $r_{\rm cool}$ (the mean mass density of distributed gas follows $\overline{\rho} \propto r^{-2}$). For this to occur, the intracluster medium must be multiphase, with a range of gas densities and temperatures at each radius existing in pressure equilibrium.

2.1 Physical conditions

A typical value for $\mathrm{d}\dot{M}/\mathrm{d}r$ is 1 $\mathrm{M_\odot\ yr^{-1}\ kpc^{-1}}$ (e.g. Thomas et al. 1987); the mean density of the hot gas is $\sim 5\times10^{-3}$ $\mathrm{cm^{-3}}$ at 100 kpc and rises inward roughly as r^{-1}, and the mean temperature drops from $kT \sim 5$ keV at 100 kpc to about 2 keV at 20 kpc. Within that last radius, the mean temperature probably stays close to the virial temperature of the galaxy. The gas pressure therefore rises inward from $nT \sim 3\times10^5$ $\mathrm{cm^{-3}}$ K at 100 kpc to $>10^6$ $\mathrm{cm^{-3}}$ K within 20 kpc. The gas pressure in our calculations is chosen to match that measured from the X-ray data of Abell 2199 at 100 kpc (Thomas et al. 1987).

The total mass of cold gas clouds within the flow determined from X-ray absorption studies is 10^{11}–10^{12} $\mathrm{M_\odot}$ (White et al. 1991). The mean excess column density measured is about 3×10^{20}–10^{21} $\mathrm{cm^{-2}}$. If the cold gas is in a population of clouds which have a thermal pressure in equilibrium with that of the surrounding hot gas, then they must be very small, with radii much less than a parsec.

2.2 The incident continuum

The spectrum emitted by the gas in cooling flows has been discussed by Johnstone et al. (1992 and references therein). For the present study we use as our base model one in which gas with one-third solar metallicity cools from $\log(T/\mathrm{K}) = 7.8$ down to $\log(T/\mathrm{K}) = 5.0$. We approximated the continuous range of temperatures by a sum of isothermal spectra (from the recently updated work of Raymond & Smith 1977), spaced at intervals of 0.1 in $\log T$.

The normalization of the cooling-flow spectrum is set by calculating the flux incident on a cloud as

$$F_{\rm cool} = \frac{L_{\rm cool}}{4\pi r_{\rm cool}^2}, \qquad (3)$$

where $L_{\rm cool}$ is given by equation (1). The model has a mass deposition rate of 100 $M_\odot$ yr^{-1} and a cooling radius of 100 kpc.

The ionizing flux increases approximately as r^{-1}, since the cooling luminosity within a given radius is proportional to that radius. Since the pressure also rises as r^{-1}, the ionization parameter, $\xi = L/nr^2$, remains approximately constant with radius. Comparing different clusters, we note that approximately $\xi \propto r_{\rm cool} T$ and the pressure at $r_{\rm cool} \propto T^{3/2}$. Inferred values of $r_{\rm cool}$ and T vary by factors of about 2 and 3, respectively, so there is a maximum range in ξ of about a factor of 6, with the value taken here being near the upper end.

Below 10^6 K, the gas cools so rapidly that it will be out of ionization equilibrium (Canizares, Markert & Donahue 1988), and the detailed shape of the components of the incident spectrum from temperatures below this value will therefore be incorrect. These components contribute only 2 per cent of the total luminosity, however, and we have ensured that the total luminosity is correct. The incident continuum is shown as the dotted line in Fig. 1(a).

The parameters of the model of the photoionized cloud within the cooling flow are given in Table 1. The model was chosen to have a gas pressure typical of regions of a cooling flow roughly 100 kpc from the centre of a massive cooling flow ($nT \approx 3\times10^5$ cm^{-3} K), and abundances one-third of solar, as inferred from X-ray studies. Table 1 lists the assumed abundances and the integrated intensity of the incident continuum. The same abundances were used in the CLOUDY model. For the present work, we restrict our investigation to these parameters. In particular, we assume that grains, magnetic fields and particle heating are not present; we will relax this assumption in a future investigation.

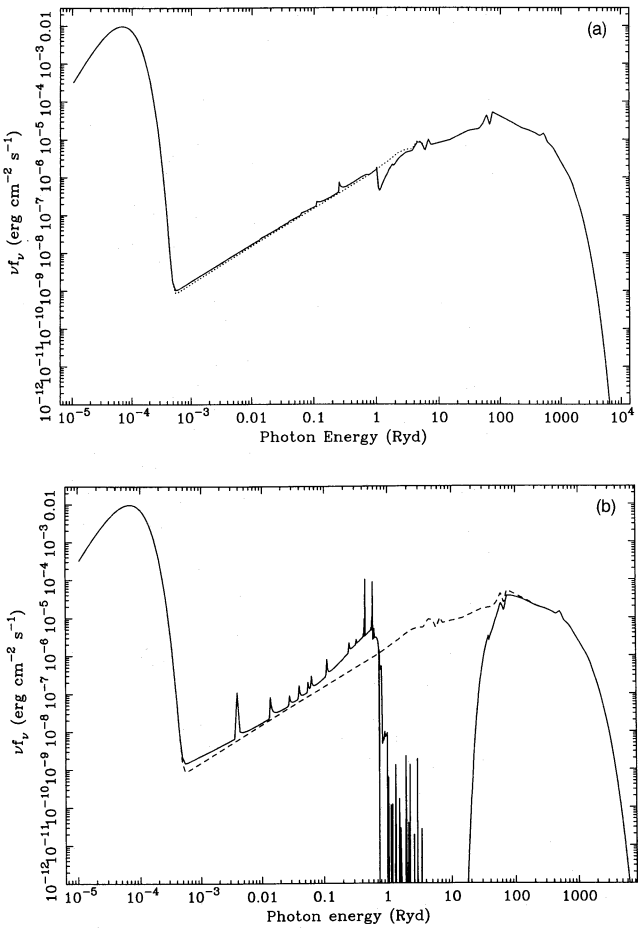

Figure 1. The continuum incident on the illuminated face of the cloud is shown as the dotted/dashed line in both Figs 1(a) and (b). (a) The solid line shows the continuum at the thermal front, where the gas changes state from the warm to the cold phase. (b) The solid line shows the continuum at the point where the calculation stops. Photon energies are given in Rydberg (1 Ry = chR_∞ = 13.605 83 eV).

3 CLOUD STRUCTURE

The modifications made to the radiative equilibrium code CLOUDY (Ferland 1992) in order to calculate the properties of cold regions exposed to an energetic X-ray continuum are described in Appendix A. In Appendix B, the predictions of this code are compared favourably with a simulation of the Orion Photo Dissociation Region (PDR), a well-studied region characterized by very low ionization, which is also approaching the fully molecular limit (Tielens & Hollenbach 1985a,b). We find our model to be no worse a fit to the observed line strengths than that of Tielens & Hollenbach (1985b).

3.1 Thermal and ionization structure

The computed structure of the irradiated cloud is shown in Figs 2 and 3, and the predicted emission-line spectrum is tabulated in Table 2. Two distinct regions can be identified in Fig. 2(a). A fairly uniform, warm outer region is separated by a 'thermal front' at a depth of 5.5×10^{15} cm [corresponding to a hydrogen column density of $\sim 3\times10^{17}$ cm^{-2} (Fig. 2b)] from a cold inner region which becomes increasingly molecular and dense with depth.

At the illuminated face of the cloud the hydrogen and carbon ionization fractions are 0.093 and 0.192, respectively; the ionization parameter is low, and no predominantly ionic region exists. Both the low level of ionization and the intermediate temperature (roughly 6000 K) make the outer regions of the cloud, before the thermal front is reached, more like the warm phase of the ISM than a conventional photoionized nebula. Fig. 2(c) shows the relative abundances of singly ionized hydrogen, carbon and silicon, and the electron fraction throughout the cloud. Conditions remain fairly uniform across this warm outer region until the thermal front is reached.

The continuum is monotonically extinguished throughout the warm outer region. For the assumed plane-parallel geometry, conditions change only because of attenuation caused by photoelectric absorption (hydrogen and helium being the dominant opacity, while carbon dominates the opacity in the Balmer continuum), continuum scattering (the cloud is optically thick to Rayleigh scattering in the region

Table 1. Parameters of the model of the cloud irradiated by the cooling flow.

$n_0(H)$[1]	38.0
$n_{Tot}T$[2]	2.9×10^5
I_0^3	1.04×10^{-4}
He[4]	8.511×10^{-2}
C	1.093×10^{-4}
N	3.010×10^{-5}
O	2.180×10^{-4}
Ne	2.745×10^{-5}
Na	5.868×10^{-7}
Mg	8.680×10^{-6}
Al	8.101×10^{-7}
Si	1.093×10^{-5}
S	5.230×10^{-6}
Ar	2.621×10^{-6}
Ca	6.584×10^{-7}
Fe	1.044×10^{-5}
Ni	5.868×10^{-7}

[1]Density of hydrogen in atom cm^{-3} at the illuminated face of the cloud. [2]Total gas pressure from all particles in cm^{-3} K. [3]Integrated intensity of cooling flow continuum above 1 Ry in erg cm^{-2} s^{-1}. [4]Abundances relative to hydrogen by number.

near 1250 Å; this process is discussed further in Appendix A), and line absorption (the Lyman–Werner bands of H_2 control the eventual formation of H_2).

The gas undergoes a radical change of state at the 'thermal front'. This occurs because the gas heating rate falls until the unstable region of the cooling function between roughly 2000 and 4000 K is reached. The heating (dashed line) and cooling functions (solid line) at a depth of 5.0×10^{15} cm (just before the thermal front is reached) are shown in Fig. 4. The figure was produced by computing a series of models in which the temperature was varied but the attenuated incident continuum left at its deduced value, which is shown as the solid line in Fig. 1(a). The heating rate does not depend on temperature in Fig. 4, a characteristic of predominantly neutral gas. (For an ionized gas, the heating rate is proportional to the recombination rate and thus decreases roughly linearly with increasing temperature.) For temperatures greater than 5000 K, the dominant coolant is the [C I] 9850-Å doublet (see Fig. 3b), while within the broad peak the dominant coolants are the [O I] 63, 147-μm, H_2 and Si II 35-μm lines. At much lower temperatures, the cooling comes mainly from the Si II 35-μm line. For temperatures below the peak at 2000 K, the cooling increases with temperature as the Boltzmann factor of the Si II line approaches unity, then falls above 2000 K due to the decreasing Coulomb focusing factor ($T^{-1/2}$). Lepp et al. (1985) discuss other aspects of the thermal stability of the warm–cold phase interface of the ISM. We ignore conduction effects across the front.

Fig. 3(a) shows the major heating agents as a function of depth. Photoionization of hydrogen and helium are the dominant heat sources, as expected for a gas photoionized by a hard continuum. At large depth the Lyman continuum is well attenuated (the continuum at the point where the calculation ends is shown as the solid line in the lower panel of Fig. 1b), and helium becomes the major heat source. The importance of helium and the photoionization of oxygen and neon as heating sources in deep regions is due to their large opacities at intermediate X-ray energies.

Fig. 3(b) shows the cooling agents as a function of depth. For the warmest regions the [C I] 9850-Å doublet dominates the cooling, giving way to [O I] 63, 147-μm, H_2 and Si II 35-μm lines across the thermal front. For regions beyond the thermal front, cooling shifts to the [C I] fine-structure lines (the 370, 610-μm doublet) and CO.

Fig. 2(d) shows that the gas becomes increasingly molecular beyond the thermal front. H_2 forms here, not via the surfaces of grains which are assumed to be absent, but through H^-. This is plentiful when compared to similar density regions in our Galaxy, because the X-rays from the cluster gas cause secondary ionization which maintains a small but important ionized fraction in the gas. Before the thermal front is reached, H_2 molecules are destroyed chiefly by discrete absorption into the Lyman–Werner bands, although collisional dissociation of the molecules is taken into account (both of these processes are discussed further in Appendix A). Beyond the front, the Lyman–Werner bands of H_2 are optically thick, and the H_2 molecules well-shielded. The predominant destruction mechanism is then high-energy photoionization and secondary-electron ionization (see also Voit 1991), which have the same effects as background Galactic cosmic rays which create the ambient level of ionization in Galactic molecular clouds and PDRs (see the discussion in Appendix A and in Tielens & Hollenbach 1985a). The carbon monoxide abundance increases with depth for similar reasons: ionization by secondary electrons and X-rays, and charge transfer with ionized helium (itself created by these two processes) are the dominant agents destroying this molecule. The water abundance is also shown, although it does not play a major role in this environment (the gas is too cold to form water efficiently in the deeper regions). CH and OH are not shown, but have abundances intermediate between CO and H_2O. The other 14 molecules included in the network have abundances generally below that of H_2O.

We terminate our calculation when the temperature falls to that of the cosmic background radiation, since the cloud properties do not change beyond this point. There, carbon monoxide is the dominant coolant, and molecular processes dominate the physical conditions. The present treatment of CO cooling is approximate (it is based on the prescription given by Hollenbach & McKee 1979). In particular, the microphysics that couples the lower rotation levels of the molecules to the background is not included. At very low temperatures, interactions between the continuum and CO will ensure that the levels are well-coupled to this continuum. The level populations will approach LTE at the background temperature for this reason. Collisions between a particle and a molecule with these level populations will act to heat the gas if the temperature is below the background, and cool the gas if the temperature is above it. The limiting case is that the gas approaches the temperature of the background. This is the final thermal state of a gas that is very well shielded from non-background radiation (this is similar to the case of CN; see the discussion in Spitzer 1977).

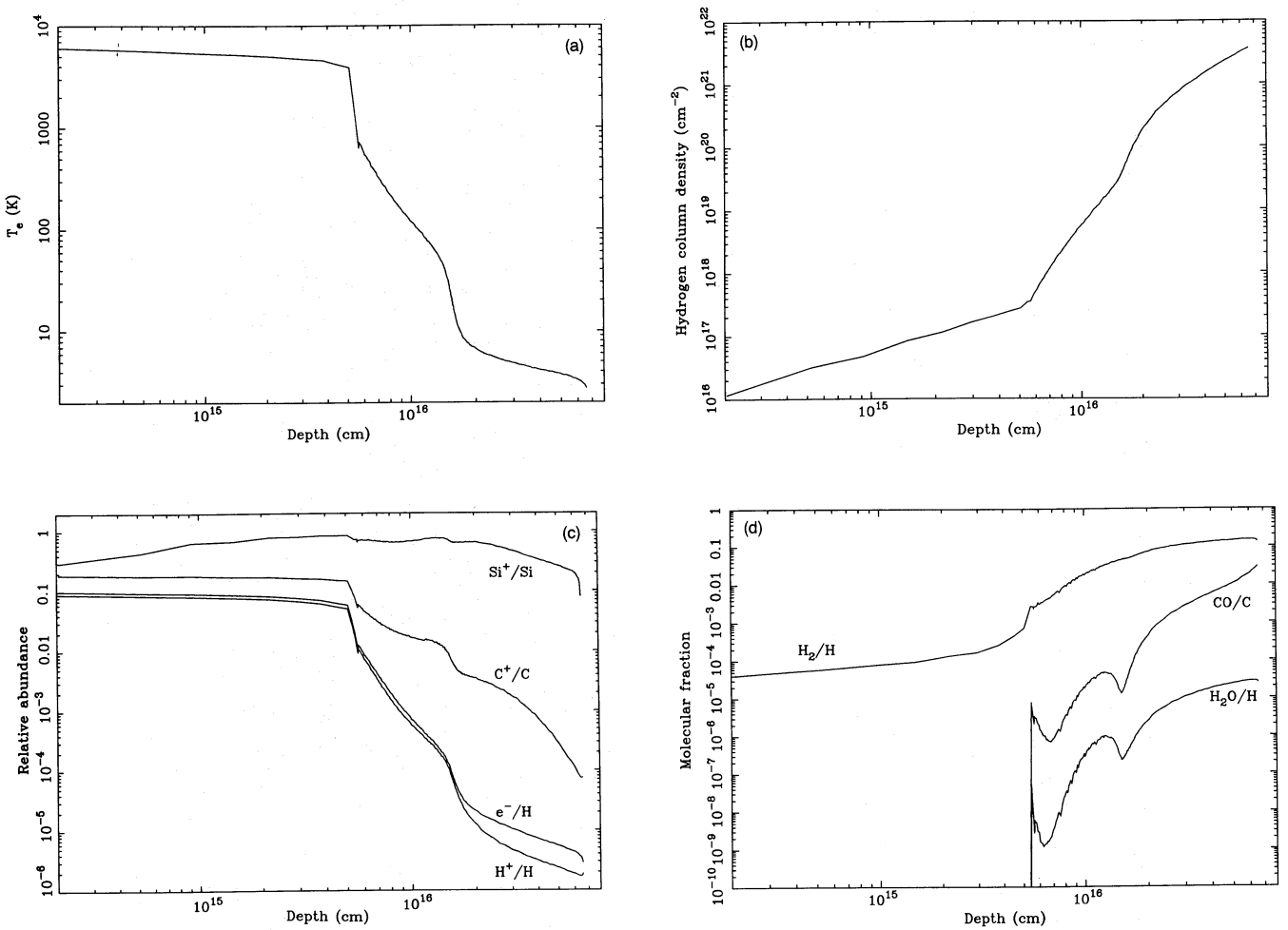

Figure 2. The temperature, column density, ionization and molecular fraction of the cloud. (a) shows the computed electron temperature as a function of the depth from the illuminated face of the cloud. (b) shows the cumulative hydrogen column density through the cloud. (c) shows the relative abundance of singly ionized hydrogen, carbon and silicon and the electron fraction. (d) shows the relative abundance of several of the important molecules in our calculation. At the illuminated face the gas is predominantly atomic or singly ionized. H_2 destruction through the carbon ionizing continuum becomes self-shielding. The H_2 molecular fraction is the ratio of the number of hydrogen molecules to the number of protons (i.e. fully molecular gas has a fraction of 0.5).

3.2 The predicted emission-line spectrum

Table 2 gives the predicted emission-line spectrum from the model cloud. Line intensities are expressed relative to Hβ, the flux of which is given. This flux corresponds to a luminosity $\sim 3\times10^{41}$ erg s^{-1}, spread over a radius of 100 kpc. In the inner 5 kpc where optical emission lines are observed in cooling-flow galaxies, we compute a luminosity of $\sim 10^{40}$ erg s^{-1} in Hβ. Although this is similar to the luminosities observed in some of the weak-lined, cooling-flow galaxies, the emergent emission-line spectrum from the irradiated cold clouds does not have the correct line ratios to explain the observed emission-line spectrum. In particular, lines of [O II] $\lambda\lambda$3727, 3729, [O III] $\lambda\lambda$4959, 5007, [N II] $\lambda\lambda$6548, 6584 and [S II] $\lambda\lambda$6716, 6731, which are commonly seen in cooling-flow galaxies, are not present in our models. Some additional heating mechanism is needed to explain these lines and the higher luminosity cooling flows. The model spectrum is dominated by very strong fine-structure lines from neutral and singly ionized species. This is largely the result of the combination of the low ionization parameter and relatively hard continuum. Some of the brighter fine-structure lines should already be detectable near the centre of cooling flows using the NASA Kuiper Airborne Observatory, while ISO will allow mapping in the fainter regions further out.

Neutral helium lines are quite strong relative to hydrogen lines for the same reason: helium can remain ionized where hydrogen is largely neutral because of its large cross-section at soft X-ray energies. The hydrogen line spectrum is far from Case B. For instance, the intensity of Hβ is enhanced by about 30 per cent above its Case B value (predicted from the level of ionization through the cloud) because of collisional excitation by both thermal and non-thermal secondary electrons. (The total column density in ionized hydrogen is about 2.5 times that expected from the ionizing photon flux for similar reasons. Note that the column density in neutral hydrogen is roughly $\sim 5\times10^4$ times that in ionized hydrogen. The neutral hydrogen would be largely undetectable by spectroscopic means, and highly optically thick at 21 cm.)

Table 2. Predicted emission-line spectrum.

$F^1(H\beta)$	2.42×10^{-7}
$H\beta$	1.00
$H\alpha$	4.26
$Ly\alpha$	21.6
H_2^2	1.14
HeI 5876Å	0.90
HeI 3889Å	0.10
HeI 10830Å	0.59
CI 9850Å	0.37
[CI] 610μm	8.61
[CI] 370μm	2.51
[CII] 158μm	1.38
[OI] 63μm	9.71
[OI] 147μm	0.34
CO (total)[3]	0.54
[SiII] 34.8μm	9.22
Fe IR[4]	0.38
[Fe II] 4μm[5]	0.26
[Fe II] 2μm[6]	0.12
[Fe II] 1μm[7]	0.12
CI 1656Å	0.22

Note: All species giving intensities greater than $0.1 \times H\beta$ are listed. [1]Emitted flux in $H\beta$ line in erg cm^{-2} s^{-1}. [2]Sum of H_2 rotational lines near 2 μm. [3]Cooling due to CO vibrational and collisional lines. [4]Sum of all infrared cooling from 6D ground state. [5]Sum of [Fe II] lines near 4 μm. [6]Sum of [Fe II] lines near 1.7 μm. [7]Sum of [Fe II] lines near 1.2 μm.

$H\alpha$ is similarly enhanced relative to $H\beta$ (the reason for this change in the Balmer decrement is discussed by Ferland & Osterbrock 1986). The intrinsic $Ly\alpha$ spectrum of the nebula is enhanced well above Case B for similar reasons. The observed spectrum is well below Case B, however (Table 2), because the line is extinguished by the background opacity of the gas (mainly photoelectric opacity of very low-ionization-potential atoms such as Si, Ca, Fe, etc.). Destruction of $Ly\alpha$ heats the gas by this mechanism as well.

4 DISCUSSION

We have shown that the cores of clouds in cooling flows are likely to be predominantly molecular and cold. The calculations presented above show that, even for an assumed grain-free mixture, photoelectric and Rayleigh scattering shielding of the innermost regions is sufficient to ensure that molecular hydrogen and carbon monoxide are abundant species. For the assumed composition (O/C greater than unity), a significant amount of oxygen remains atomic, which further contributes to the cooling.

The physical conditions in the asymptotic core of the cloud can be estimated without recourse to numerical calculations. Hydrogen and carbon will be fully molecular, and the gas kinetic temperature will be at or slightly above the cosmic background temperature. The microphysics which guarantees the latter is as follows. The radiation field of the cosmic background has a large photon occupation number at wavelengths longward of the peak in the energy distribution. Absorption and stimulated emission will force the level populations to their LTE values, appropriate for the temperature of the cosmic background. The gas kinetic temperature will then approach this temperature. Were the gas hotter than the background, then collisions would tend to lose kinetic energy to the internal rotation energy of the molecule, which would then be overpopulated relative to the LTE value. This overpopulation would soon be corrected by enhanced induced emission by the background. The opposite would occur if the gas temperature were to fall below the background; collisions with well-coupled molecules would be supra-elastic and heat the gas. In the end, the gas kinematic temperature approaches the background closely, in the absence of significant high-energy heating.

4.1 Fate of the cold gas

If we assume that the cores are fully molecular and at the background temperature [$T_{MWB} = 2.756(1+z)$ K], then we can estimate the Jeans mass in a straightforward manner as a function of the gas pressure at the illuminated face of the cloud, which we parametrize as $P_s = nT$, where n is the total number density and T the temperature. Assuming constant gas pressure, the density at the core of the cloud is then

$$\rho_{core} = 1.405 \times 10^{-19} \left(\frac{P_s}{10^5}\right) (1+z)^{-1} \text{ g cm}^{-3}, \quad (4)$$

the Jeans length is

$$\lambda_J = 1.8 \times 10^{17} (1+z) \left(\frac{P_s}{10^5}\right)^{-1/2} \text{ cm}, \quad (5)$$

and the Jeans mass is

$$M_J = 0.22 (1+z)^2 \left(\frac{P_s}{10^5}\right)^{-1/2} M_\odot. \quad (6)$$

This is $\sim 0.1\ M_\odot$ for our model cloud. The column density giving a Jeans mass is

$$N_J \approx 10^{22} \left(\frac{P_s}{10^5}\right)^{1/2} \text{ cm}^{-2}. \quad (7)$$

The maximum fragmentation mass given by equation (6) corresponds to relatively low-mass stars. Clouds with column densities exceeding N_J presumably form into such stars, while those with lower column densities remain to be detected through X-ray absorption. In fact, this estimate only gives the mass of the initial fragment in the hierarchical fragmentation process (Rees 1976). Subsequent fragments will be of much lower mass, ensuring that a large population of substellar mass clumps (less than about a tenth of a solar mass) results. It therefore seems likely that a large fraction of the condensed gas can form into low-mass stars. The mean mass of stars formed at earlier epochs could, however, be higher.

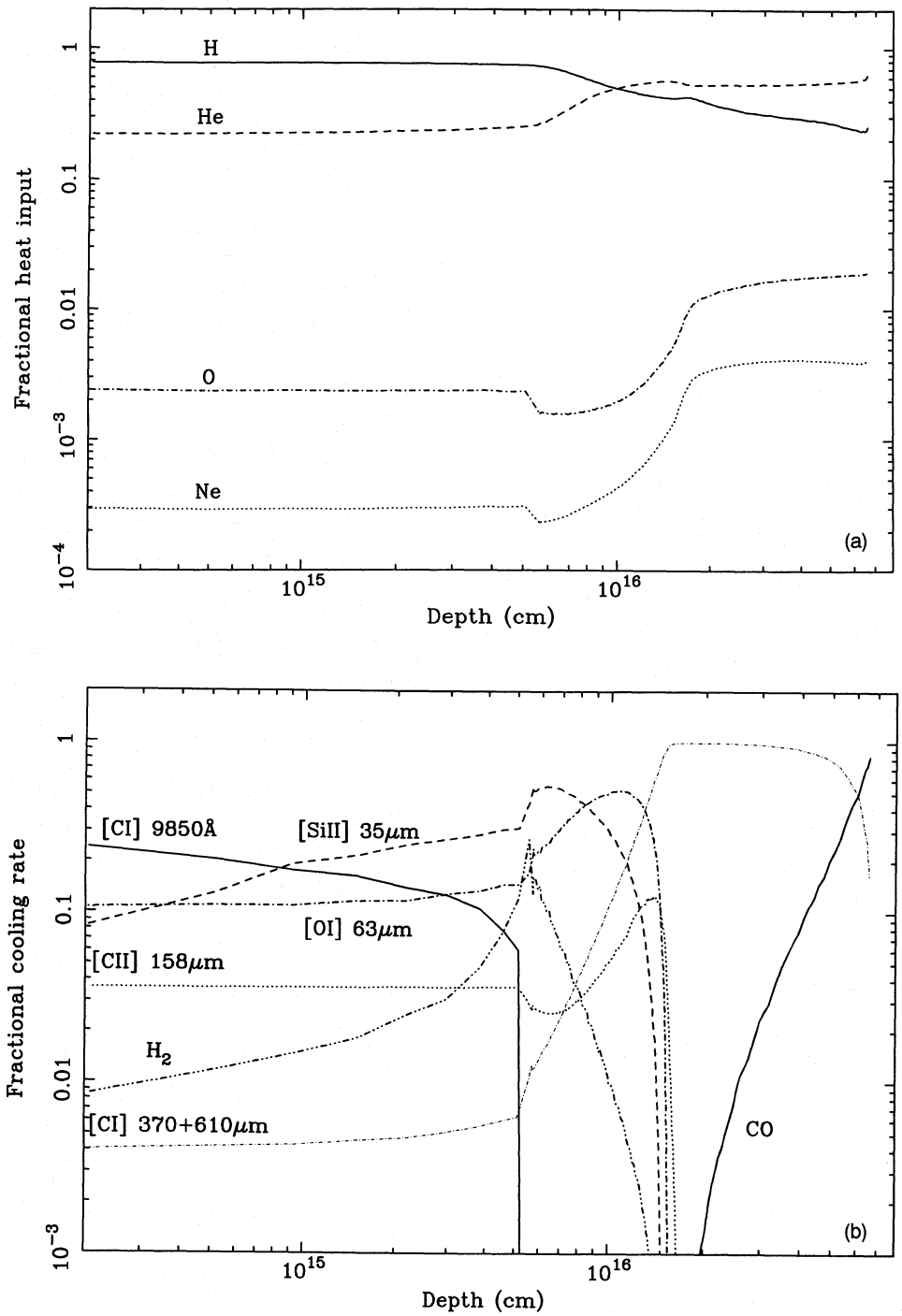

Figure 3. The fractions of heating (a) and cooling (b) due to various agents are shown as a function of depth into the cloud. Photoionization of hydrogen and helium dominate the heating of the cloud. Deep regions are well shielded, with mainly relatively hard X-rays being present. Here, photoionization of oxygen and neon becomes more important because of their large cross-sections at X-ray energies. In the warm regions of the cloud the main coolants are the [C I] 9850-Å doublet, giving way to the Si[II] 35-μm, H_2 and [O I] 63-μm lines near the thermal front. Finally, the [C I] 370, 610-μm lines and CO bands take over as lower temperatures are reached.

5 CONCLUSIONS

X-ray-irradiated, dust-free clouds in a cooling flow have a thin, partially ionized outer layer and a molecular core which drops to the temperature of the cosmic background radiation. Hydrogen is significantly molecular throughout much of the core; carbon monoxide and other molecular species only become important constituents in the deepest regions.

Such clouds will be difficult to detect in emission, since they reprocess the absorbed X-ray continuum into optical and infrared lines, which will be faint since the emission is spread over a region that has a radius of 100 kpc. The

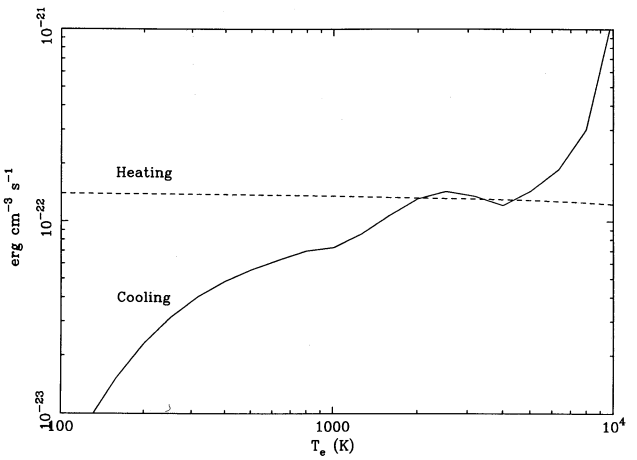

Figure 4. The heating and cooling functions at the thermal front. This plot shows the results of a series of calculations, in which the temperature was varied but the continuum was held fixed at a form appropriate for a depth just before the thermal front occurs. Heating (the dashed line) does not depend on temperature, since the gas is predominantly neutral. Cooling (the solid line) increases due to the temperature dependence of the [Si II] 35-μm line, and eventually saturates when the Boltzmann factor reaches unity. The rapid rise in cooling above 6000 K is due to the [C I] 9850-Å doublet.

clouds are best detected by X-ray absorption, although they can also absorb a significant fraction of the UV continuum from a background quasar or central nucleus.

The Jeans mass of the cores of such clouds can be much less than a solar mass, making the formation of condensed objects of substellar mass in cooling flows a plausible hypothesis.

ACKNOWLEDGMENTS

GJF thanks the NSF for continued support, most recently through grant AST 90-19692. ACF thanks the Royal Society for support.

REFERENCES

Baldwin J. A. et al., 1991, ApJ, 374, 580
Bergeron J., Souffrin S., 1971, A&A, 11, 40
Black J. H., 1978, ApJ, 222, 125
Canizares C. R., Markert T. H., Donahue M. E., 1988, in Fabian A. C., ed., Cooling Flows in Clusters and Galaxies. Kluwer, Dordrecht, p. 63
Cowie L. L., Binney J., 1977, ApJ, 215, 723
Crosas M., Weisheit J. C., 1993, MNRAS, 262, 359
Dalgarno A., Roberge W. G., 1979, ApJ, 233, L25
Doughty N. A., Fraser P. A., McEachran R. P., 1966, MNRAS, 132, 255
Dove J. E., Mandy M. E., 1986, ApJ, 311, L93
Dove J. E., Rusk A. C. M., Cribb P. H., Martin P. G., 1987, ApJ, 318, 379
Draine B. T., Salpeter E. E., 1979, ApJ, 231, 177
Draine B. T., Sutin B., 1987, ApJ, 320, 803
Edge A. C., Stewart G. C., Fabian A. C., 1992, MNRAS, 258, 177
Elitzur M., 1991, Astronomical Masers. Kluwer, Dordrecht
Fabian A. C., Nulsen P. E. J., Canizares C. R., 1982, MNRAS, 201, 933
Fabian A. C., Nulsen P. E. J., Canizares C. R., 1984, Nat, 310, 733
Fabian A. C., Nulsen P. E. J., Canizares C. R., 1991, A&AR, 2, 191
Ferland G. J., 1992, HAZY, a Brief Introduction to CLOUDY 84, University of Kentucky Center for Computational Sciences Internal Report
Ferland G. J., Mushotzky R., 1984, ApJ, 286, 42
Ferland G. J., Osterbrock D. E., 1986, ApJ, 300, 658
Ferland G. J., Persson S. E., 1989, ApJ, 347, 656
Gavrila M., 1967, Phys. Rev., 163, 147
Gredel R., Lepp S., Dalgarno A., 1987, ApJ, 323, L137
Gredel R., Lepp S., Dalgarno A., Herbst E., 1989, ApJ, 347, 289
Habing H. J., 1968, Bull. Astron. Inst. Neth., 19, 421
Hollenbach D. J., McKee C. F., 1979, ApJS, 41, 555 (HM79)
Hollenbach D. J., McKee C. F., 1989, ApJ, 342, 306 (HM89)
Hoyle F., 1953, ApJ, 118, 513
Jaffe W., 1990, A&A, 240, 254
Janev R. K., Langer W. D., Evans K., Post D. E., 1987, Elementary Processes in Hydrogen-Helium Plasmas. Springer-Verlag, Berlin
Johnstone R. M., Fabian A. C., Edge A. C., Thomas P. A., 1992, MNRAS, 255, 431
Lambert D. L., Pagel B. E. J., 1968, MNRAS, 141, 299
Latter W. B., Black J. H., 1991, ApJ, 372, 161
Lenzuni P., Chernoff D. F., Salpeter E., 1991, ApJS, 76, 759 (LCS91)
Lepp S., Shull J. M., 1983, ApJ, 270, 578
Lepp S., McCray R., Shull J., Woods D., Kallman T., 1985, ApJ, 288, 58
Lites B. W., Mihalas D., 1984, Solar Phys., 93, 23
Low C., Lynden-Bell D., 1975, MNRAS, 176, 367
Mihalas D., 1978, Stellar Atmospheres. W. H. Freeman, San Francisco
Mushotzky R. F., 1992, in Fabian A. C., ed., Clusters and Superclusters of Galaxies. Kluwer, Dordrecht
Pradhan A., Zhang H. L., 1993, ApJ, 409, L77
Puy D., Alecian G., Le Bourlot J., Leorat J., Pineau des Forêts G., 1993, A&A, 267, 337
Raymond J. C., Smith B. W., 1977, ApJS, 35, 419
Rees M. J., 1976, MNRAS, 176, 483
Richer H. B., Crabtree D. R., Fabian A. C., Lin D. N. C., 1993, AJ, 105, 877
Roberge W. G., Jones D., Lepp S., Dalgarno A., 1991, ApJS, 77, 287
Sarazin C. L., 1986, Rev. Mod. Phys., 58, 1
Sarazin C. L., O'Connell R. W., 1983, ApJ, 258, 552
Shull M. J., van Steenberg M., 1985, ApJ, 298, 268
Spitzer L., 1977, Physical Processes in the Interstellar Medium. Wiley, New York
Stecher T. P., Williams D. A., 1967, ApJ, 149, 29
Thomas P. A., Fabian A. C., Nulsen P. E. J., 1987, MNRAS, 228, 973
Tielens A. G. G. M., Hollenbach D. J., 1985a, ApJ, 291, 722 (TH85)
Tielens A. G. G. M., Hollenbach D. J., 1985b, ApJ, 291, 747 (TH85)
Voit G. M., 1991, ApJ, 377, 1158
White D. A., Fabian A. C., Johnstone R. M., Mushotzky R. F., Arnaud K. A., 1991, MNRAS, 252, 72
White R. E., Sarazin C. L., 1987, ApJ, 318, 612
Wishart A. W., 1979, MNRAS, 187, 59
Wolfire M. G., Tielens A., Hollenbach D., 1990, ApJ, 358, 116
Zygelman B., Dalgarno A., 1990, ApJ, 365, 239

APPENDIX A: NUMERICAL DETAILS

A1 Continuous opacities

A1.1 Rayleigh scattering

Clouds with neutral-hydrogen column densities greater than $\sim 10^{23}$ cm^{-2} are optically thick to Rayleigh scattering at

wavelengths near Ly α, and this process is a major scattering opacity source at short wavelengths for grain-free environments.

Rayleigh scattering cross-sections given by Gavrila (1967) are used, joined with expressions for the radiative damping wings of Lyman lines (Mihalas 1978). For wavelengths longward of 1410 Å, a power-law fit to Gavrila's quantal calculations is used:

$$\sigma_{\rm Ray} = 8.41\times10^{-25}\,\varepsilon^4 + 3.37\times10^{-24}\,\varepsilon^6 + 4.71\times10^{-22}\,\varepsilon^{14}\ {\rm cm}^{-2}, \quad \text{(A1)}$$

where $\varepsilon \equiv \nu/cR_\infty$ is the photon energy in Ry. This fit is accurate to typically a per cent, with occasional errors as large as 4 per cent.

For wavelengths between 1410 Å and the Lyman limit, radiative broadening of the Lyman lines is assumed (Mihalas 1978):

$$\sigma_{\rm Ray} = \sum_{i=2}^{4} \left(\frac{q_e^2 f_{1,i}}{m_e c}\right) \frac{\Gamma/4\pi}{(\nu-\nu_{1,i})^2}\ {\rm cm}^2, \quad \text{(A2)}$$

where Γ is the reciprocal lifetime of the upper level i, and the sum is over the first four Lyman lines. This expression gives cross-sections in excellent agreement with Gavrila (1967) for these wavelengths.

A2 The hydrogen network

The treatment of the major hydrogen molecules (i.e., H_2, H_2^+, H_3^+ and H^-) is based on Lambert & Pagel (1968), Black (1978), Lites & Mihalas (1984), Hollenbach & McKee (1979, 1989, hereafter HM79 and HM89), Tielens & Hollenbach (1985a,b, hereafter TH85), Lenzuni, Chernoff & Salpeter (1991, hereafter LCS91), Wolfire, Tielens & Hollenbach (1990), Crosas & Weisheit (1993) and Puy et al. (1993).

A3 H^-

Ferland & Persson (1989) describe the portions of the molecule network pertaining to the H^- balance. In dust-free environments H_2 forms by associative detachment of H^-, following formation of the negative hydrogen ion by radiative attachment. The H^- ion is the pace-setter for the formation of molecular hydrogen in a grain-free environment, and so its abundance must be determined with some precision.

A3.1 Radiative attachment

This is the most important creation mechanism for H^- at low densities when three-body processes are negligible;

$$H^0 + e^- \Rightarrow H^- + \gamma. \quad \text{(A3)}$$

For temperatures greater than 10^4 K, the rate coefficient is evaluated by numerically integrating the photodetachment cross-section over frequency:

$$\alpha_{\rm rad}(T) = P^*(H^-) \int_{\nu_0}^{\infty} \alpha_\nu \frac{8\pi\nu^2}{c^2} \times \exp(-h\nu/kT)\,{\rm d}\nu\ ({\rm cm}^3\ {\rm s}^{-1}), \quad \text{(A4)}$$

where cross-sections computed by Wishart (1979) and spline interpolation are used. These cross-sections are in excellent agreement with the velocity operator bound–free cross-sections tabulated by Doughty, Fraser & McEachran (1966). The energy interval between the photodetachment threshold at 0.055 502 Ry and ~1.8 Ry is divided into roughly 100 cells with logarithmically increasing width, and the integration is carried out as a straightforward sum.

This method is not numerically expedient for very low temperatures, where the energy bandwidth of the integral is small and a much finer frequency grid would be required. Rather, the integration was carried out using spline interpolation and 32-point Gaussian quadrature, integrating over factors of 2 in $h\nu/kT$. The results were then fitted with a set of power laws. The rate coefficients (${\rm cm}^{-3}\ {\rm s}^{-1}$) can be approximated by

$$\alpha(T_e) = \begin{cases} 8.934\times10^{-18}\,T^{0.505} & 1\ {\rm K} \le T < 31.62\ {\rm K} \\ 5.159\times10^{-18}\,T^{0.664} & 31.62\ {\rm K} \le T < 90\ {\rm K} \\ 2.042\times10^{-18}\,T^{0.870} & 90\ {\rm K} \le T < 1200\ {\rm K} \\ 8.861\times10^{-18}\,T^{0.663} & 1200\ {\rm K} \le T < 3800\ {\rm K} \\ 8.204\times10^{-17}\,T^{0.393} & 3800\ {\rm K} \le T \le 10^4\ {\rm K}. \end{cases} \quad \text{(A5)}$$

These approximations fit the exact numerical results with a mean deviation of 0.7 per cent, and a largest error of 2.05 per cent, over the indicated temperature range. Other details concerning the creation and destruction of H^- are given by Ferland & Persson (1989).

A4 HeH^+

Rates for radiative association for He^+ and H^+ to form HeH^+ are taken from Zygelman & Dalgarno (1990).

A5 H_2

The hydrogen chemistry network includes the ion-molecules H_2, H^-, H_2^+ and H_3^+. All of the chemical reactions involving H_2 described by HM79, TH85, HM89 and LCS91 have been incorporated in the present treatment. Rather than go into these details, which are well presented in these papers, we only outline details of how some of the processes have been implemented.

A5.1 Associate detachment of H^-

The process

$$H^- + H \Rightarrow H_2 + e \quad \text{(A6)}$$

is the main H_2 formation mechanism in low-density, grain-free regions, and is treated as in Ferland & Persson (1989). At temperatures of interest here (~10^3 K), the rate for H_2 formation by this process is set by the rate for radiative association to form H^-, and is of order 10^{-15} ${\rm cm}^3\ {\rm s}^{-1}$ (see above).

A5.2 Catalysis on grain surfaces

The process

$$2H + {\rm grain} \Rightarrow H_2 + {\rm grain} \quad \text{(A7)}$$

is a competitive H_2 formation process when grains are present. The rate coefficient is taken from Hollenbach & McKee (1979). Defining the fraction of atoms that form molecules as

$$f_a = [1 + 10^4 \exp(-600/T_{gr})]^{-1}, \quad \text{(A8)}$$

the rate coefficient is given by

$$\alpha_{gr}(H_2) = 3\times10^{-18} \frac{\sqrt{T_e} A_{gr} f_a}{1 + 0.04\sqrt{T_{gr}+T_e} + 0.002\, T_e + 8\times10^{-6} T_e^2}, \quad \text{(A9)}$$

where A_{gr} is the grain abundance relative to the ISM value, and T_e and T_{gr} are the electron and grain temperatures, respectively. The grain temperature is determined self-consistently, including radiative and collisional heating and cooling, as described by Baldwin et al. (1991).

At $T_e = 10^3$ K and $T_{gr} = 100$ K (representative values of the gas and grain temperatures in regions near a H^0–H_2 interface) the rate coefficient is $\sim 4\times10^{-18}$ cm^{-3} s^{-1}. For most conditions of interest here, radiative association is at least a competitive H_2 formation mechanism. The ratio of the two processes (referred to as the H^- and grain H_2 formation routes) is then

$$\frac{r(H^-)}{r(\text{grain})} = \frac{n_e \alpha(H^-)}{n_H \alpha(\text{grain})} \approx \frac{n_e}{n_H} 250, \quad \text{(A10)}$$

i.e., the H^- route is faster for conditions of moderate ionization ($n_e/n_H > 4\times10^{-3}$) even when grains are present. When grains are absent (or deficient) the H^- route dominates.

A5.3 Excited-atom radiative association

Rates for the process

$$H(n=2) + H(n=1) \Rightarrow H_2 + h\nu \quad \text{(A11)}$$

are taken from Latter & Black (1991).

A5.4 Excited molecular dissociation

Rates for the process

$$H_2(v \geq 4) + e^- \Rightarrow (H_2^-)^* \Rightarrow H + H^- \quad \text{(A12)}$$

are given in Janev et al. (1987, their process 2.2.17), and these have been adopted by Lenzuni et al. (1991) and Crosas & Weisheit (1993) in their work on high-density gas. Tests show that this process is, if taken at face value, by far the fastest destruction mechanism for molecular hydrogen under ISM conditions.

The process outlined by Janev et al. (1987) involves an electron capture by H_2 into vibrationally excited levels ($4 \leq v \leq 9$). The process is fast at low temperatures because the energy barrier is small, and the excited levels have large populations at laboratory densities. The process proceeds much more slowly at ISM densities, however, because excited levels have populations below their LTE values. The situation is thus similar to that described by Dalgarno & Roberge (1979). We have modified the Janev et al. (1987) process using the physics outlined by Dalgarno & Roberge.

A5.5 Discrete absorption into Lyman and Werner bands

Line absorption and excitation leading to dissociation through the vibrational continuum,

$$H_2 + h\nu \Rightarrow H_2^* \Rightarrow 2H + h\nu, \quad \text{(A13)}$$

is the dominant H_2 destruction mechanism in regions where photodissociation (by photons with $h\nu > 14.7$ eV) and photoionization (with $h\nu > 15.4$ eV) do not occur (Stecher & Williams 1967).

Photodissociation through the Lyman–Werner bands occurs through a large number of transitions between 1109 Å and the Lyman edge for a region shielded by atomic hydrogen (i.e., no radiation shortward of 912 Å). Individual H_2 electronic transitions are optically thick for sufficient column densities, and eventually the H_2 becomes self-shielding. H_2 then becomes the dominant hydrogen species.

Photodissociation through the Lyman–Werner bands is included, using the approximations outlined by TH85. The incident radiation field is taken as the mean over the energy interval 1109–912 Å (appropriate for photoexcitation into the $B^1\Sigma_\mu^+$ electronic state). This quantity is then reposed in terms of the Habing (1968) radiation field, which is the quantity used by TH85. H_2 self-shielding is included, using escape probabilities and the deduced optical depth, again adopting the approximations described by TH85.

A5.6 Photoionization to H_2^+

Photons with energies greater than 15.4 eV produce H_2^+ via

$$H_2 + h\nu \Leftrightarrow H_2^+ + e^*. \quad \text{(A14)}$$

This process creates H_2^+ and heats the gas. Photo-absorption cross-sections are taken from the compendium of Janev et al. (1987).

A5.7 Collisional dissociation by H^0, He^0 and e^-

The rate coefficient for the forward process, collisional dissociation by the species S (one of H^0, He^0 or e^-),

$$H_2 + S \Rightarrow 2H + S, \quad \text{(A15)}$$

is taken from Dove & Mandy (1986, dissociation by H^0), Dove et al. (1987, dissociation by He^0) and Janev et al. (1987, dissociation by electrons). These can be important destruction mechanisms only for warm regions of the ISM because of the large binding energy of H_2 ($\sim 50\,000$ K).

The reverse reactions are included via detailed balance. Three-body formation of H_2 is important only for very high densities ($n \gg 10^{10}$ cm^{-3}).

A5.8 H_2 cooling

Cooling due to collisional excitation of vibration-rotation levels of H_2 is treated using the analytic fits given in Lepp & Shull (1983). Both H_2–H and H_2–H_2 collisions are included.

A5.9 H_2 heating

Many electronic excitations eventually decay to excited vibration-rotation levels within the ground electronic state, and these can then heat the gas following collisional de-excitation. The scheme outlined by TH85 is again used.

A6 The heavy-element network

The heavy-element chemistry network includes the molecules CH, CH^+, OH, OH^+, CH_2^+, CO, CO^+, H_2O, H_2O^+, H_3O^+, O_2 and O_2^+. The heavy-element network, the hydrogen network described above, and the hydrogen–helium ionization balance network, are solved self-consistently. Of the 12 molecules in the heavy-element network, only CO develops a significant population under most circumstances.

A6.1 Collisional processes

The collision network described by Hollenbach & McKee (1989) is included (the original implementation of the network was based entirely on this work). Their approximations for the temperature dependence of the rate coefficients are used.

A6.2 Photochemical processes and heating

Rates for photochemical reactions of the form $h\nu + XY \Rightarrow X + Y$ are largely taken from the compendium of Roberge et al. (1991). These are posed in terms of the average interstellar radiation field. They have been incorporated by taking the depth-dependent continuum, renormalizing this to the average interstellar radiation field, and then using the coefficients given by Roberge et al.

An exception to this prescription is CO, which can become a major opacity source. Photodissociation is treated by numerically integrating over the continuum (with a threshold of 12.8 eV), using the photodissociation cross-section given by HM79.

Photodissociation heats the gas if the internal energy of the daughters is small. The kinetic energy is taken to be $\langle h\nu - DE \rangle$, where DE is the dissociation energy, and the mean is over the portion of the Balmer continuum that is active. Again, an exception is CO (the most important, since it is the only heavy molecule that becomes optically thick), where the heating is evaluated by numerically integrating over the attenuated incident continuum.

A6.3 Cooling

Cooling due to collisional excitation of vibration-rotation levels of CO, CH, OH and H_2O is treated using the scheme outlined by HM79. Of these, CO is the most important.

A6.4 Fine-structure line heating and cooling

Atomic-ionic fine-structure lines are often optically thick. In all cases these transitions are transferred using escape probabilities, by determining level populations including both collisional and radiative processes (see, for example, Elitzur 1991). Line masing can sometimes occur, and again is treated using escape probabilities.

FIR fine-structure lines can act to heat the gas if an intense IR continuum is present. This can occur for either a region near warm dust, or gas at large redshift. If η is the photon occupation number of the attenuated incident continuum, then the rate at which atoms are excited from the ground level is given by $\eta\varepsilon A_{ul}$, where ε is the line escape probability. A fraction $C_{ul}/(A_{ul} + C_{ul})$ of these radiative excitations is converted into heat by collisional de-excitation. The net heating due to this process is then

$$G_{FIR} = n_l \eta \varepsilon_{lu} A_{ul} \left(\frac{C_{ul}}{C_{ul} + \varepsilon_{lu} A_{ul}} \right) h\nu \text{ erg cm}^{-3} \text{ s}^{-1}, \qquad \text{(A16)}$$

where n_l is the density of the ground level. This process can be a major heating mechanism for well-shielded gas.

A7 Cosmic rays and suprathermal electrons

The collisional and heating effects of the suprathermal secondary electrons following inner-shell photoionization are treated using standard assumptions (Bergeron & Souffrin 1971; Shull & van Steenberg 1985; Voit 1991). The treatment of cosmic ray processes is described by Ferland & Mushotzky (1984). Following TH85, we assume that 8 eV of heat is deposited for each H_2 ionization by a cosmic ray. Relative rates are taken from HM89. The result of this is a secondary ionization rate, which must then be multiplied by scale factors which account for the relative collision cross-section for each species relative to hydrogen. These are taken from HM89 and TH85.

Secondary electrons also produce a diffuse background of the electronic H_2 line which can photodissociate most molecules. This is treated using the scaling rule of Gredel, Lepp & Dalgarno (1987) and Gredel et al. (1989).

A8 Grain surface recombination

Positive ion recombination on grain surfaces proceeds at a rate $n_{ion} n_H \alpha_{gr}$, where the recombination coefficient is taken from Draine & Sutin (1987, their equation 5.15). For a standard grain size distribution and non-positive grain charges (true for deeper regions of the cloud), this rate coefficient is of order $\sim 5.8 \times 10^{-13}\, T^{-0.5}$ cm^3 s^{-1}. This process is included for all ions considered in the calculation when grains are present, using the full equation given by Draine & Sutin. This process only competes with radiative recombination when the electron fraction is well below the levels considered in this paper.

APPENDIX B: THE ORION PDR

As a test of the physics incorporated into the code, a model with parameters similar to those of the standard photodissociation region (PDR) model of TH85 was computed. This model is far more extreme than those considered in this paper, in the sense that *no* ionizing (above 13.6 eV) radiation exists. Ionization is by the incident Balmer continuum produced by the Trapezium stars, and cosmic rays (given their Galactic background value), while heating is by this continuum and the intense FIR continuum due to warm dust. A major difference between the calculations described above and the Orion PDR calculation is the dominant role played by grains. In the Orion PDR, grains provide the opacity which shields the molecular regions, photoionization of the grains is by far the dominant heating source of the gas, and H_2 formation on grain surfaces is important.

The TH85 standard model was recomputed. As far as possible, their parameters (table 2 of Tielens & Hollenbach 1985a) were used. The boundary conditions used in our calculation are not identical to HM85 for several reasons.

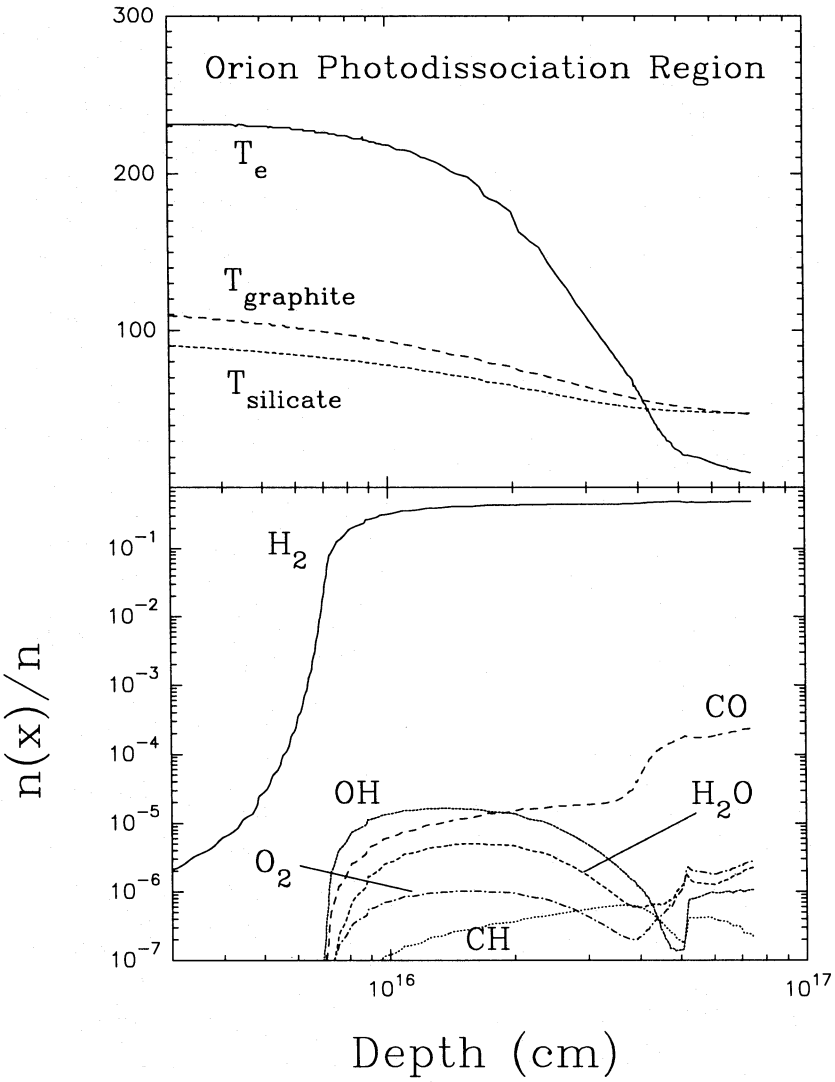

Figure B1. The Orion PDR. The temperature and molecular content of the Orion Photodissociation Region are shown as a function of depth from the illuminated face of the cloud. The upper panel shows the temperature of the electrons and the two grain species included in the calculation. The lower panel shows the molecular density normalized to the total particle density. The calculation stops when hydrogen and carbon become fully molecular.

The treatment of grain charging, photoionization, heating and cooling in the present code is described by Baldwin et al. (1991). The grain properties, such as the grain cross-section, work function, photoelectric yield, and gas heating efficiency, are not identical. Of these, the grain cross-section in the ultraviolet and the heating efficiency of grain photoionization are the most crucial (see Baldwin et al. 1991 for a complete description of our formalism). Orion grain opacities (chosen to match the large ratio of total to selective extinction observed in the Trapezium stars) are used, and are somewhat smaller in the UV than standard ISM grains. A closed geometry, in which the scattering part of the cross-section is discounted, is assumed (see Baldwin et al.). The incident continuum has a Rayleigh–Jeans slope with an intensity at 1400 Å set to 10^5 times the Habing (1968) value.

Fig. B1 shows the computed PDR structure, and Table B1 gives the predicted line intensities. The general structure is similar to that found by TH85, but there are significant differences which are attributable to the different treatments

Table B1. The Orion Photodissociation Region[1].

Line	Observed	TH85	Cloudy
O I 63 μm	5-8 (-1)	9.4 (-1)	3.5 (-1)
O I 145 μm	3-8 (-2)	4.0 (-2)	7.8 (-3)
C II 158 μm	5-9 (-2)	3.3 (-2)	2.8(-2)
C I 610 μm	8.4 (-5)	4.4 (-5)	1.0 (-4)
C I 370 μm		2.3 (-4)	2.5 (-4)
Si II 34.8 μm		2.0 (-2)	5.7 (-3)
Fe II IR		1.6 (-2)	9.1(-4)
CO (total)		9.7 (-3)	9.2(-3)

[1]Orion PDR standard model of Tielens & Hollenbach (1985). All lines are expressed as intensities (erg cm^{-2} s^{-1}).

of grain processes. In general, the temperatures are similar, but the peak temperature in our calculation is roughly 240 K, smaller than the peak found by TH85. This occurs because the fraction of the incident photon energy that goes into heat of the freed photoelectron produced by grain photoionization is smaller in our treatment, and because of our smaller UV cross-section. Tests show that an increase in the assumed photoelectron heat fraction by as little as 20 per cent can cause the temperature to increase to values *higher* than those found by HM85. The predicted line intensities are sensitive to such details, because the PDR reprocesses only a small fraction of the incident continuum. In our simulation of the Orion PDR, only ≈ 0.06 per cent of the total incident continuum was reprocessed into lines by the point where the calculation stopped. As a result, the predictions are sensitive to details of the grain physics, rather than to global properties. Other (less important) reasons for the differences include a different shape of the incident continuum [a continuum appropriate for the Rayleigh–Jeans tails of a hot star's energy distribution rather than the deduced Habing (1968) ISM continuum], and the chemistry network is completely independent. These networks are generally thought to have an accuracy of about a factor of 2 because of uncertainties in the molecular collision data base.

Table B1 lists the line spectrum predicted by the simulation, together with the range of observed values from the Orion PDR, and the predictions of the standard HM85 model (these were taken from HM85). The agreement between the two calculations is reasonable (generally within the factor of 2 uncertainty inherent in a calculation dominated by grains and molecules). The Fe II infrared lines employ the recent collision strengths in Pradhan & Zhang (1993). The higher excitation potential lines (O I 63 μm, Si II 34.8 μm, and the Fe II infrared lines) are weaker because the gas is generally cooler, for the reasons described above.